On inverting solar coronal vector magnetic fields from infrared observations

Trials and Tribulations

Alin R. Paraschiv

High Altitude Observatory, NCAR | UCAR

AIRA Seminar, April 2023

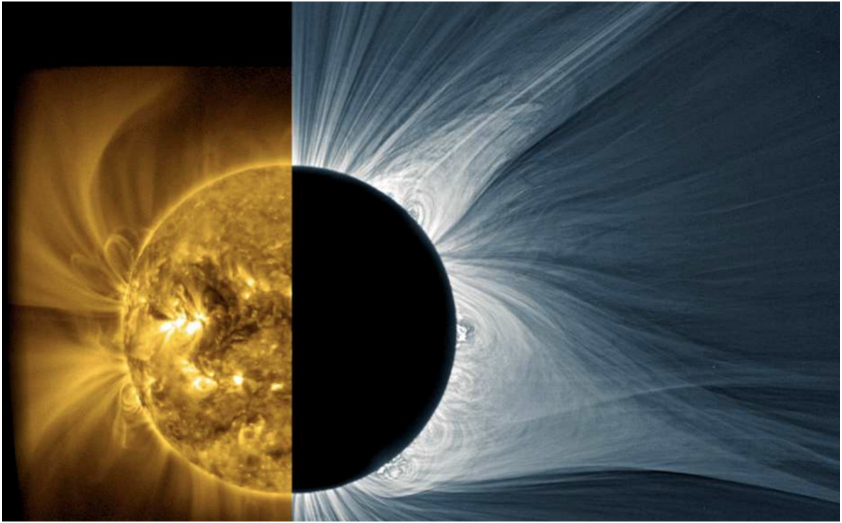

Sun's Corona extending into interplanetary space. The low density, luminosity, and yet unexplained temperature complicate the observational interpretation.

Why measure magnetic fields?

- What are the root causes of coronal heating, dynamics and flaring?

Need to measure non potential and in general **non**-force-free magnetic energy ($\mathbf{j}\times\mathbf{B}$).

Requires measurements of B(r, t) on short lengths and timescales.
$\rightarrow$ High resolution instrument like DKIST

- What is the root cause of the magnetic solar cycle?

Need to measure the magnetic helicity over solar cycle scales ($\int \mathbf{AB}dV$).

Requires measurements of B(r, t) on longer lengths and timescales.
$\rightarrow$ Synoptic instrument like CoMP/uCoMP or COSMO

Why measure magnetic fields?

More precisely:
- Nature of waves and their propagation in the corona.
- Turbulence and SW acceleration in the lower corona.
- Diagnostic of off-limb magnetic structures.
- Pre and post-eruptive CME structures.
- Theoretical studies on coronal polarization.
- Many others...

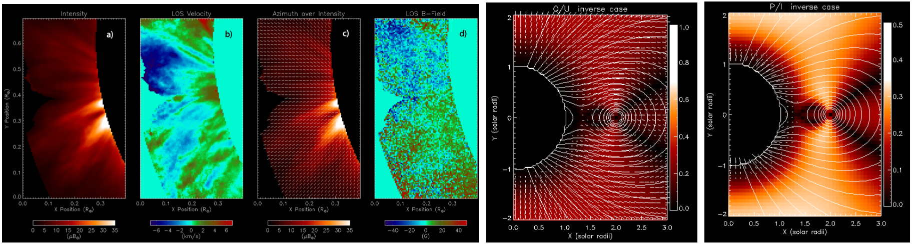

Adapted from: Tomczyk et. al, 2008, SolPhys

Definitions:

- Conventions for directions are:
  X - Along the line of sight. (Integrated in most 2D projections)
  Y - Horizontal; E-W direction.
  Z - Vertical: N-S direction

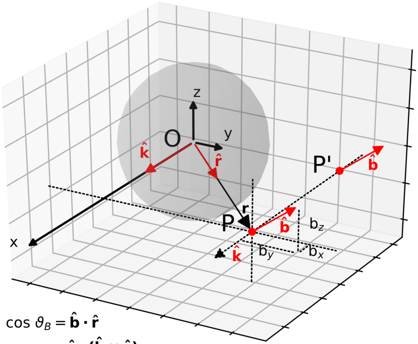

$\cos\vartheta_B = \hat{\mathbf{b}}\cdot\hat{\mathbf{r}}$

$\cos\varphi = \hat{\mathbf{x}}\cdot(\hat{\mathbf{b}}\times\hat{\mathbf{z}})$

$\cos\Theta_B = \hat{\mathbf{k}}\cdot\hat{\mathbf{b}}$

$\cos\boldsymbol{\vartheta} = \hat{\mathbf{k}}\cdot\hat{\mathbf{r}}$

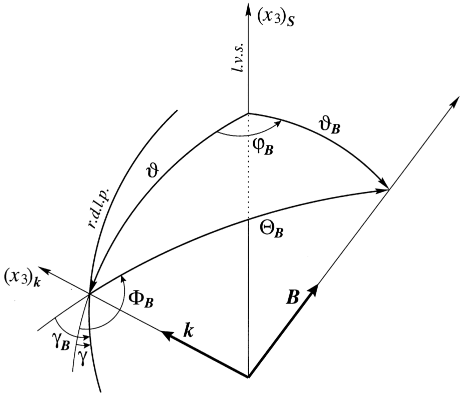

Adapted from: Casini & Judge 1999, ApJ
Judge, Cassini, & Paraschiv, 2021, ApJ

Definitions:

- Atomic alignment due to anisotropic radiation fields.
- Corona is reasonably approximated when probing the Zeeman (weak field) & Hanle (saturated regime) effects.

$$\boxed{I_1} = I_{01} + \sqrt{\frac{9}{8}}\boxed{I_{01}}\boxed{\sigma_{01}^2}(\cos^2\boxed{\theta_B} - \frac{1}{3})$$ Measurement

$$\boxed{Q_1} = -\sqrt{\frac{9}{8}}I_{01}\boxed{\sigma_{01}^2}\sin^2\theta_B\cos(2\boxed{\Phi_B})$$ Unknown

$$\boxed{U_1} = -\sqrt{\frac{9}{8}}I_{01}\boxed{\sigma_{01}^2}\sin^2\theta_B\sin(2\boxed{\Phi_B})$$

$$\boxed{V_1} = -\sqrt{\frac{9}{8}}I_{01}\boxed{\omega_B}\cos\boxed{\theta_B}(\sqrt{2} + \boxed{\sigma_{01}^2})$$

Plowman, 2014

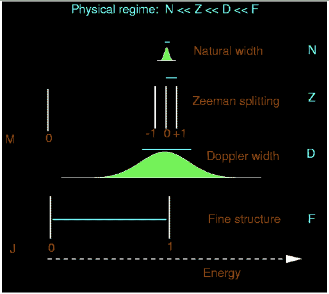

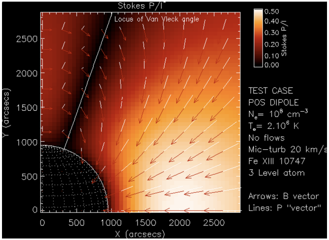

$$V/I \approx k\,B\cos(\Theta_B)\,\frac{dI}{d\lambda}\ \text{(Zeeman)}$$

$$\Phi_B \approx \frac{1}{2}\arctan\frac{U}{Q}\ \text{(Hanle)}$$

$\rightarrow$ DEGENERACIES!!!

- Target strong infrared lines formed in coronal regime
  - \+ Better seeing
  - \+ Lower scattering
  - \+ Telescope optics
  - \+ Dark sky
  - \+ Zeeman sensitivity $\sim \lambda$
  - 0- Many transitions in theory only
  - 0- Detectors ($$$)
  - \- Thermal emission from many sources
  - \- Atmospheric extinction
  - \- Cryogenic

Judge 1998

Ion	Wavelength (μm)
Fe XIV	0.530 ✓
Fe X	0.637 ✓
Fe XI	0.789 ✓
Fe XIII	1.0747 ✓
Fe XIII	1.0798 ✓
Si X	1.430 ✓
S XI	1.920
Si IX	2.584
Fe IX	2.855
Mg VIII	3.028
Si IX	3.929 ✓
Mg VII	5.502
Mg VII	9.031
Fe XI	6.081[a]
Ni XIII	19.3[a]

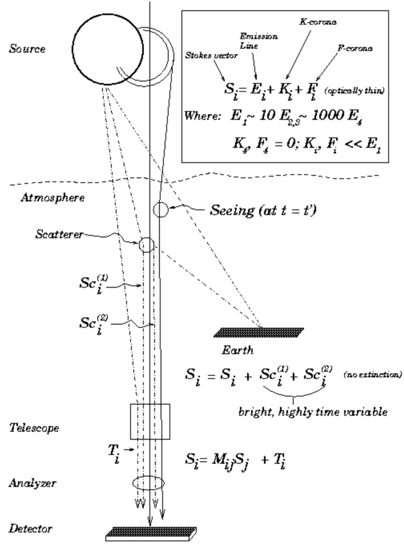

Ground Infrared spectroscopy at 1000-4000 nm

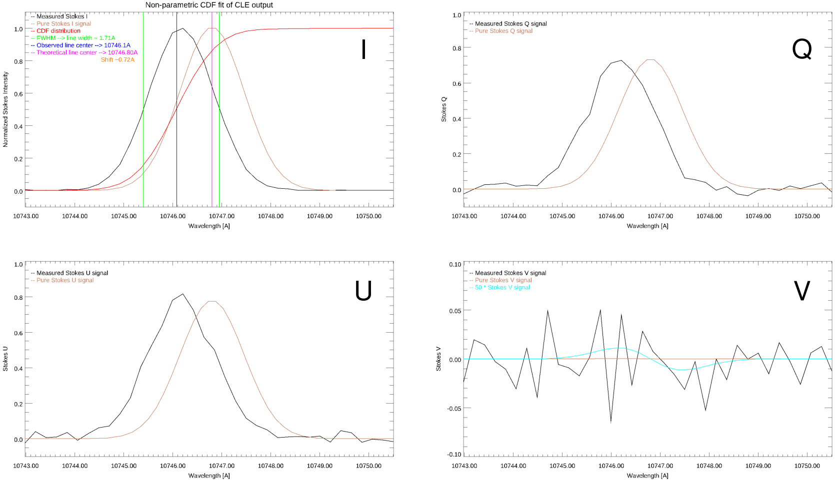

- Ions: Fe XIII 1074.7nm, 1079.8nm, Si X 1430.1nm, Si IX 3934.3nm.
- Emission might not be well fitted by parametric fitting.
- Stokes V is hard to recover.

10000 **I** ~ 10-1000 **QU** ~ 1-10 **V**

Identifying suitable atomic and molecular absorption spectra

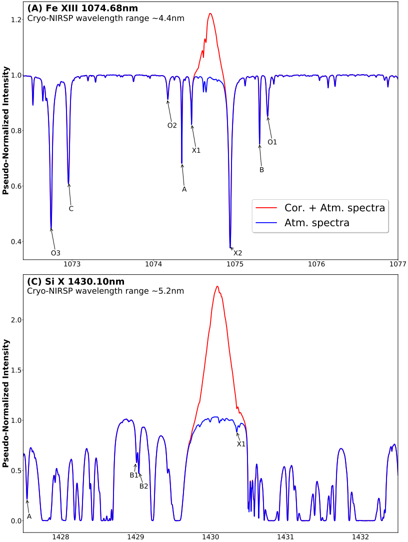

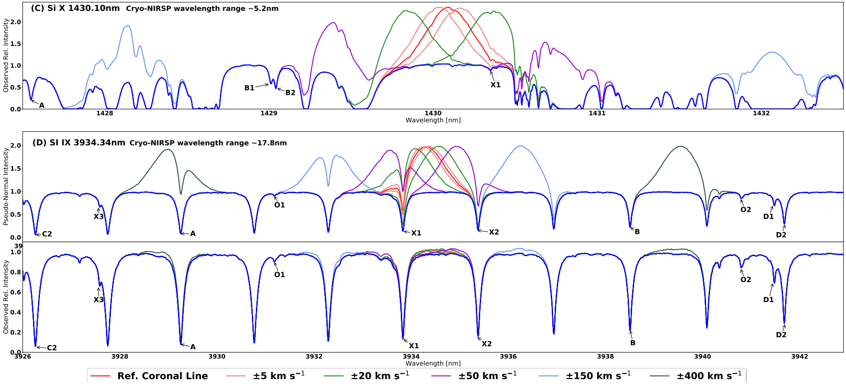

- Absorption lines will influence the integration of coronal emission lines.
- Higher outflow regions might require manual calibrations.
- The Si X wavelength region is particularly problematic.

Cor. Line & Wave.	ID	Cal. Line	Source	Wave.	CDF Wave. Range	Rel. I	Comment
Fe XIII 1074.68nm	O3	Si I	ASD	1072.74nm	1072.58nm - 1072.92nm	0.44	Very strong line; too close to slit wavelength margin
	C	C I	ASD	1072.95nm	1072.84nm - 1073.12nm	0.60	Strong absorption line
	O2	H_2O	HITRAN	1074.15nm	1073.96nm - 1074.32nm	0.91	Very weak line.
	A	H_2O	HITRAN	1074.35nm	1074.24nm - 1074.44nm	0.68	Strong absorption. Blend of two water lines.
	X1	Fe I	ASD	1074.46nm	1074.40nm - 1074.52nm	0.82	Weak line, unusable due to blend with cor. Fe XIII line
	X2	Si I	ASD	1074.94nm	1074.80nm - 1075.10nm	0.38	Strong line, unusable due to blend with cor. Fe XIII line
	B	Fe I	ASD	1075.30nm	1075.20nm - 1075.37nm	0.75	Not very prominent but might be usable
	O1	C I	ASD	1075.40nm	1075.31nm - 1075.46nm	0.85	Weak line; possible blend issue
Fe XIII 1079.79nm	A	Fe II	ASD	1078.30nm	1078.20nm - 1078.40nm	0.69	Strong absorption line
	B	Si I	ASD	1078.45nm	1078.32nm - 1078.58nm	0.63	Strong absorption line
	C	Si I	ASD	1078.68nm	1078.48nm - 1078.96nm	0.39	Very strong line
	X1	H_2O	HITRAN	1079.60nm	1079.56nm - 1079.70nm	0.89	Weak line. Very weak HITRAN S.
	-	-	-	-	-	-	Unusable due to blend with cor. Fe XIII line
	X2	H_2O	HITRAN	1079.95nm	1080.32nm - 1080.40nm	0.41	Strong line. Blend of two water lines.
	-	-	-	-	-	-	Unusable due to blend with cor. Fe XIII line
	O1	H_2O	HITRAN	1080.37nm	1080.16nm - 1080.56nm	0.88	Weak line; Strong HITRAN S.
	O2	Ne I	ASD	1080.63nm	1080.56nm - 1080.72nm	0.91	Very weak line
	D2	H_2O	HITRAN	1081.08nm	1080.72nm - 1081.52nm	0.56	Strong absorption 2-line set.
	D1	Mg I	ASD	1081.11nm	1080.72nm - 1081.52nm	0.43	Strong absorption 2-line set; treat as pair
	O3	Fe I	ASD	1081.83nm	1081.64nm - 1082.04nm	0.77	Moderately strong line; close to slit wavelength margin.
Si X 1430.10nm	A	Fe I	ASD	1427.50nm	1427.48nm - 1427.62nm	0.21	Separable line in tough range; needs specialized fitting procedure.
	B1	H_2O	HITRAN	1429.01nm	1428.83nm - 1429.14nm	0.47	Pair of close lines, fit together.
	B2	H_2O	HITRAN	1429.04nm	1428.83nm - 1429.14nm	0.57	
	X1	Fe I	ASD	1430.30nm	1430.29nm - 1430.34nm	-	Not usable due to overlap
Si IX 3934.34nm	C1	CH_4	HITRAN	3926.02nm	3925.48nm - 3927.08nm	0.71	couple with N_2O band.
	C2	N_2O	HITRAN	3926.26nm	3925.48nm - 3927.08nm	0.06	Molecular absorption to couple with C1
	X3	CH_4	HITRAN	3928.68nm	3928.62nm - 3928.72nm	0.67	Not usable due to proximity to N_2O molecular band
	A	N_2O	HITRAN	3929.25nm	3928.12nm - 3930.28nm	0.08	Molecular absorption band;
	O1	N_2O	HITRAN	3931.17nm	3931.00nm - 3931.40nm	0.90	Weaker N_2O line.
	X1	N_2O	HITRAN	3933.83nm	3933.32nm - 3936.52nm	0.13	Absorption band; not usable due to overlap
	X2	N_2O	HITRAN	3935.38nm	3933.32nm - 3936.52nm	0.15	Absorption band; not usable due to overlap
	B	N_2O	HITRAN	3938.50nm	3938.12nm - 3938.92nm	0.22	Molecular absorption band
	O2	SO_2	HITRAN	3940.80nm	3940.44nm - 3941.24nm	0.84	Weak line. Weak S in HITRAN. Blend with weak water line.
	D1	CH_4	HITRAN	3941.47nm	3941.16nm - 3942.12nm	0.69	Blend of two methane lines. Couple with N_2O band.
	D2	N_2O	HITRAN	3941.66nm	3941.16nm - 3942.12nm	0.29	N_2O Molecular band for D1.

Aatiya Ali et. al, 2022, ApJ

Geometry and symmetries: Dima & Schad, 2020 special degeneracy

• Casini & Judge, 1999 (ApJ), Plowman, 2014 (ApJ), and Dima & Schad, 2020(ApJ), incrementally work towards this problem.

• Dima & Schad, 2020, ApJ offer a purely analytical solution to the discussed problem. Compelling 1-line and 2-line discussions are presented.

• The authors showed that some 2-line combinations will contain degenerate information based on the F atomic factor:

$$F=\frac{3}{4}[J(J+1)-J_0(J_0+1)-2](g_u-g_l).$$

For example : $$\begin{array}{lll} \text{Fe XIII} & ^3P_1 & \rightarrow {}^3P_0, \;\; \lambda = 1.0747\mu m, \;\; F=0 \\ \text{Fe XIII} & ^3P_2 & \rightarrow {}^3P_1, \;\; \lambda = 1.0789\mu m, \;\; F=0 \end{array}$$

• The authors suggested replacing one line with an $F\neq 0$ counterpart:

$$\text{Si X} \quad {}^2P^o_{3/2} \quad \rightarrow {}^2P^o_{1/2}, \;\; \lambda = 1.430\mu m, \;\; F=0.5$$

• The problem comes from both the unpolarizable nature of the J=0 level (for Fe XIII 1.0747μ transition) and the identical Landé factors of the J=1 and J=2 levels, in standard LS coupling conditions (in the case of the Fe XIII 1.0789μ transition).

• The Θ_B orientation is given by: $$\sin^2\Theta_B = \pm\frac{2}{3}\frac{F_1L_1V_2 - F_2L_2V_1}{\overline{g_2}V_1(I_2\pm L_2) - \overline{g_1}V_2(I_1\pm L_1)}$$

• The analytical solutions are degenerate in sets of 4.

How can we infer magnetic fields with CLEDB?

• The atomic LS coupling approximation is not accurate. Large scale computations of Lande G factors of ions of interest will update the F factors of lines of interest (Dima & Schad, 2020; Schiffmann et al. 2021.).
• Observation geometry is crucial. In using additional information when compared with purely analytical inversions, we can match one voxel with an apparent height, leading to a less ambiguous Θ_B estimation, that is not dependent on F. Aditionally, using lines of the same ion is desirable as we avoid calculating dynamical ratios of $\mathcal{A}$ (Judge, Casini, & Paraschiv, 2021).

CLEDB (Paraschiv & Judge, 2022) is a python coronal spectro-polarimetry package developed as part of the NSO Community Science Program Level-2 data effort, with the goal of helping heliophysics users with interpreting novel observations like the ones from the DKIST Cryo-NIRSP spectrograph and uCoMP coronagraph.

It is available online: https://github.com/arparaschiv/solar-coronal-inversion

The package is at the stage of initial release, and should be considered in development. Validation is currently non-trivial. Any contributions and suggestions are welcome!

Geometry and symmetries: Azimuth and Field Strength

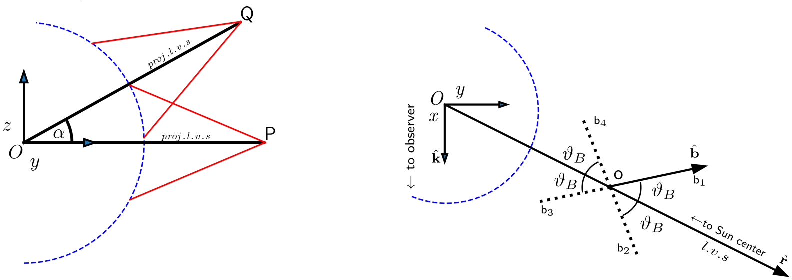

(a) Plane of the sky (POS) zy; $x = 0$

(b) Ecliptic plane xy; $z = 0$

- The alignment solutions σ_0^2 depend only on the distance from the limb. Conditions in points Q and P are equivalent in terms of σ_0^2. The Stokes QU profiles at Q can be rotated towards P. After a matching solutions are found, the profiles are derotated.
- To simplify the solution fitting, we use the CLEDB database to compute entries for $|B| = 1G$, only! Matching solutions are scaled via the ratio of V_{obs}/V_{db}.

Geometry and symmetries: Height

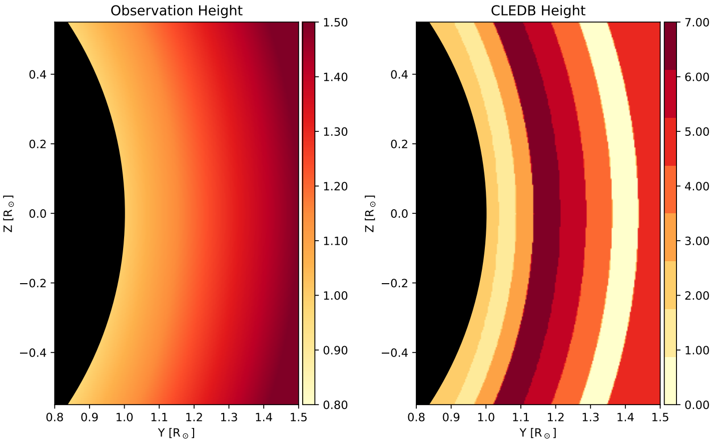

- Database entries are stored and retrieved efficiently.

The CLEDB atomic Database

- A database for Stokes IQUV profiles is calculated using CLE to cover all possible points in an $\mathbf{r} = (x, y, z)^T$ space.

- Theoretically we should be solving over a parameter space consisting of: $x, y, z, T_e, n_e, \mathcal{A}, B, \Theta_B, \Phi_B, v_x, v_T$.

- We can reduce calculations to just: $x,\ n_e,\ \vartheta,\ \varphi$.

- Example of CLEDB configuration: Number of calculations for each of 81 y entries $N_C = n_x \cdot n_{n_e} \cdot n_\varphi \cdot n_\vartheta = 7.9 \times 10^8$

quantity	number	range
n_e (electron density in cm^{-3})	$n_{n_e} = 10$	[200.0 100 50.0 15.0 5.0 2.5 1.0 0.5 0.1 0.01]$n_0(r)$
y-axis (radial, units $R_\odot$)	$n_y = 81$	$1.0 \rightarrow 1.256$
x-axis (LOS, units $R_\odot$)	$n_x = 60$	$-1.5 \rightarrow 1.5$
φ (azimuth in $z = 0$ plane)	$n_\varphi = 180$	$0 \rightarrow 2\pi$
ϑ (polar angle from +ve $z-$axis)	$n_\vartheta = 90$	$0 \rightarrow \pi$

CLE *is a Fortran spectral synthesis code for magnetic dipole lines developed by P. Judge and R. Casini. A novel code PyCELP developed by T. Schad and G. Dima exists. It is not yet tested/integrated with CLEDB.*

CORONAL FIELD DATABASE INVERSION - SIMPLIFIED MODULE SCHEME

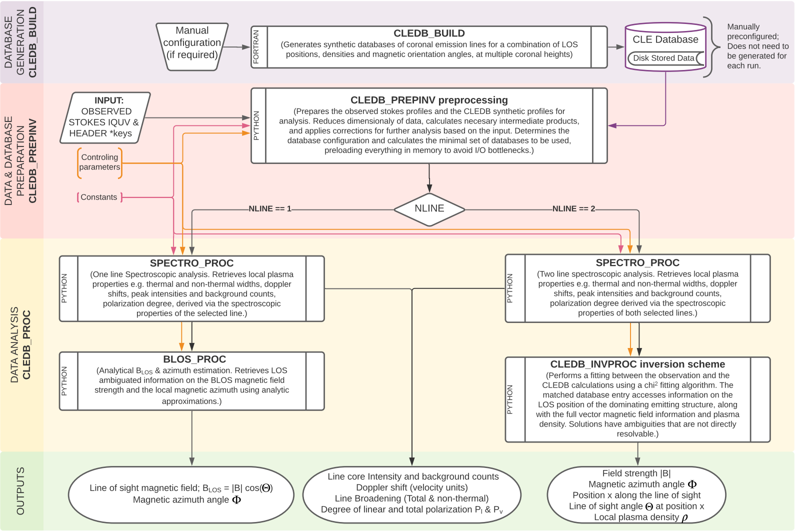

DATABASE GENERATION DIAGRAM (CLEDB_BUILD)

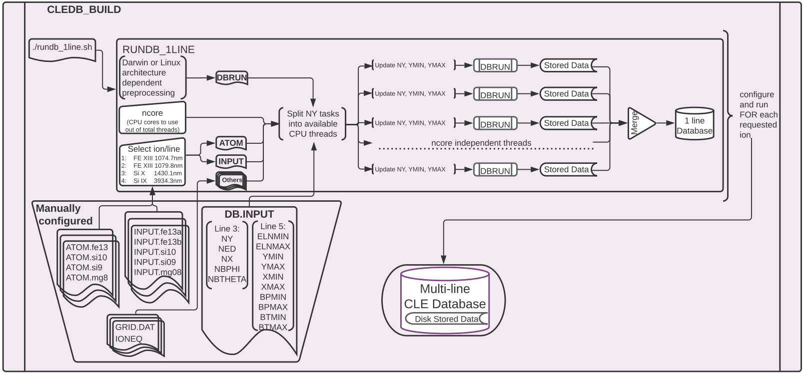

DATA PRE-PROCESSING DIAGRAM (CLEDB_PREPINV)

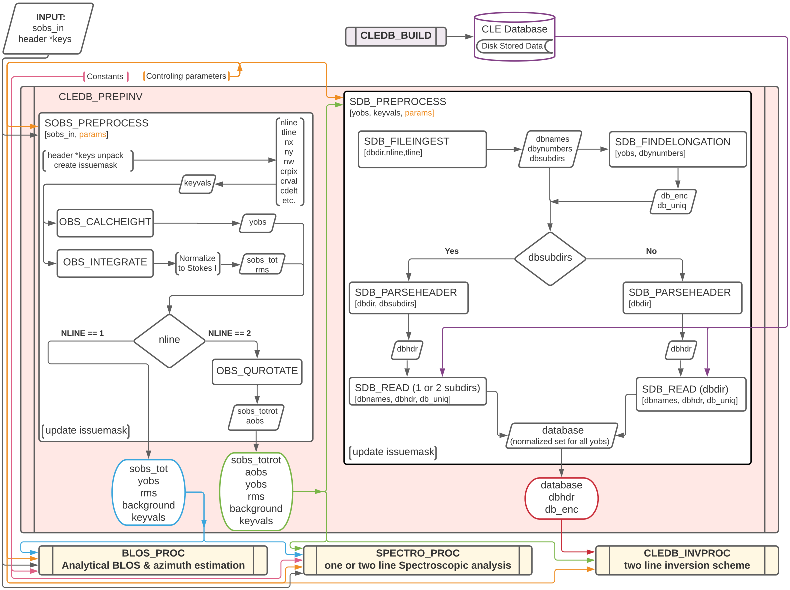

DATA ANALYSIS DIAGRAM (CLEDB_PROC)

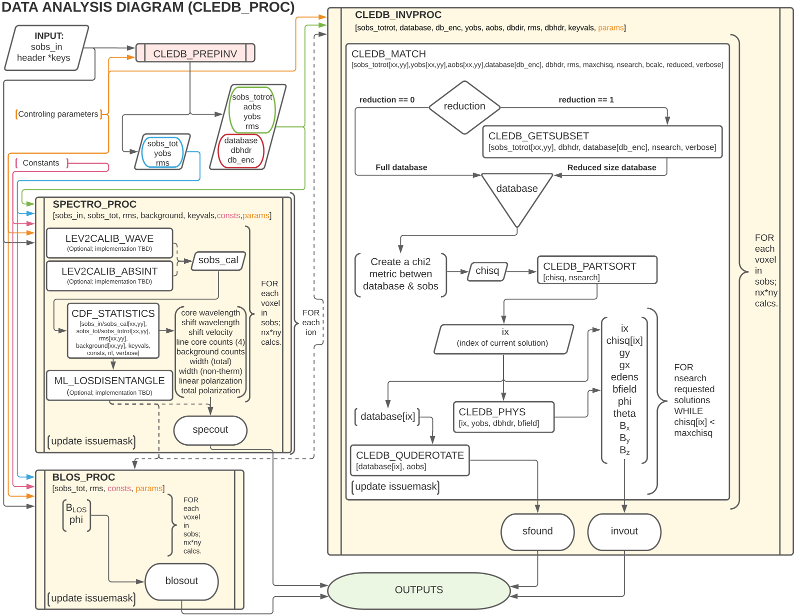

Output products

1. Calibrations and spectroscopy:

Stokes IQUV line core intensity and background counts
Doppler Shifts
Total line width
Non-thermal line width
Linear degree of polarization
Total degree of polarization

2. Magnetic field products:

A. 1-line observations → LOS magnetic field

$B_{LOS} = |B| \cos(\Theta_B)$ (see Plowman 2014, ApJ; Dima & Schad, 2020 ApJ)
Magnetic azimuth (Φ_B)

B. 2-line observations → Vector magnetic fields (in addition to A)

Magnetic field strength $|B|$
LOS magnetic component (Θ_B)
LOS position of dominant emitting structure
Plasma density (n_e)
$|\mathbf{B}|$ together with Θ_B and Φ_B are also projected to a cartezian plane; e.g. B_x, B_y, B_z

Paraschiv & Judge, 2022, SolPhys

Simplified fake observations: LOS retrieval

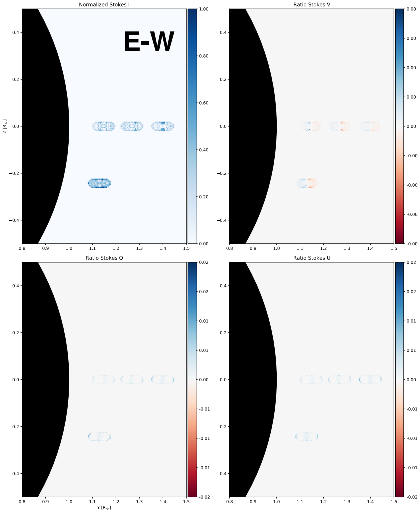

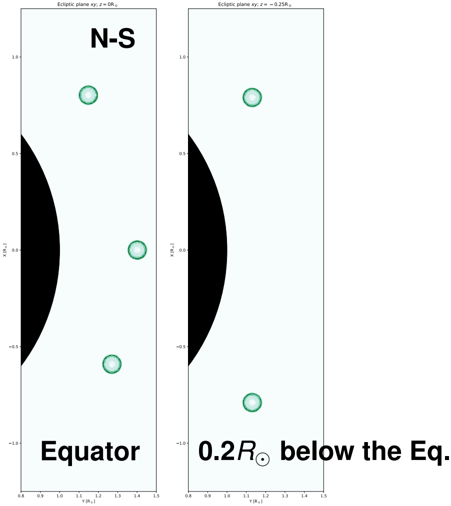

Simplified fake observations: LOS retrieval

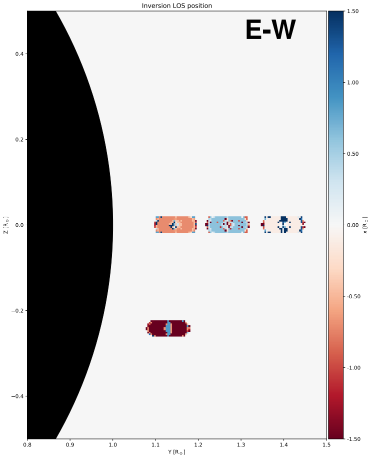

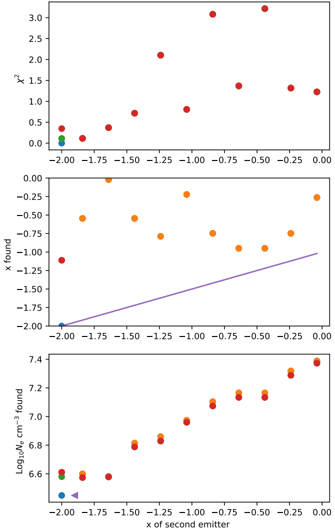

Simplified fake observations: 3 large-scale dipoles

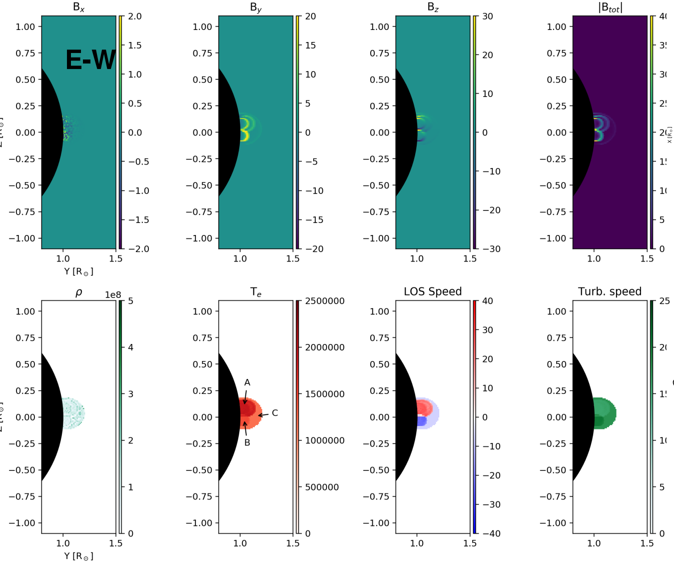

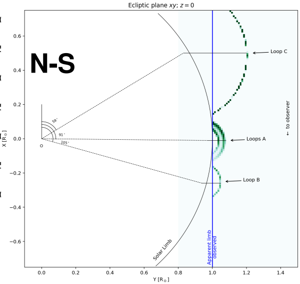

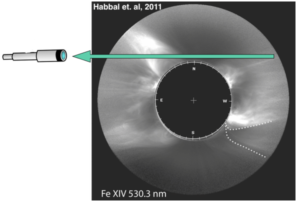

CLE Spectral Synthesis

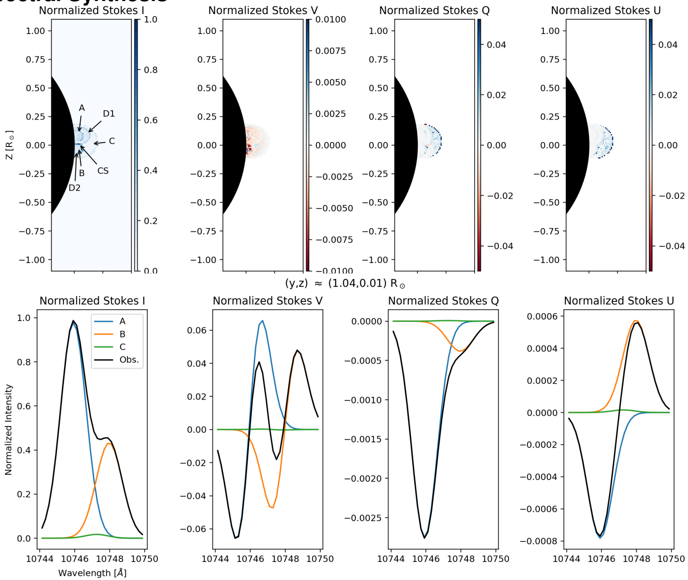

Simplified fake observations: CLEDB Line of Sight B estimation

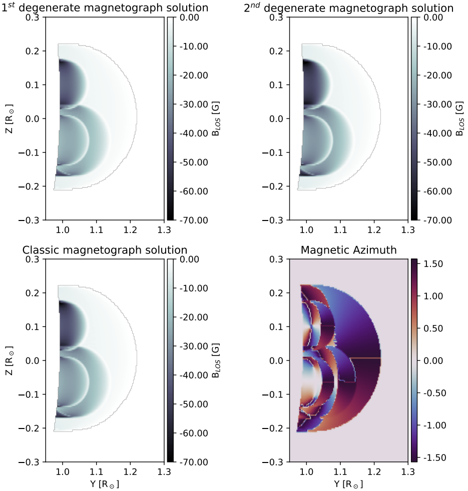

- For 1-line B LOS estimations, we employ the solution offered by Dima & Schad, 2020, alongside a classic magnetograph estimation:

$$B_{LOS}^{ob} = \frac{h}{\mu_B}\left[\frac{-V}{\overline{g}(I \pm L) \pm \frac{2}{3}F\frac{L}{\sin^2\Theta_B}}\right]$$

- Different interpretations are produced based on the input line F factor. One solution closely matched the input in the case of F=0.

Example: A Single Point Solution

Index	χ^2	n_e	H	D	|B|	Φ_B	Θ_B	B_x	B_y	B_z
5982696	2.12e-2	8.10	1.18	-0.52	6.0	108.3	72.8	-1.85	5.47	1.72
6669594	2.12e-2	8.05	1.18	0.55	6.0	253.3	108.9	-1.63	-5.47	-1.93
5990814	2.13e-2	8.10	1.18	-0.52	-6.0	289.4	108.9	-1.93	5.47	1.93
6661476	2.13e-2	8.05	1.18	0.55	-6.0	72.2	72.8	-1.71	-5.52	-1.72
5982606	3.65e-2	8.10	1.18	-0.52	6.8	106.6	72.8	-1.88	6.28	2.02
6669684	3.65e-2	8.05	1.18	0.55	6.8	255.0	108.9	-1.68	-6.28	-2.29
5982697	5.64e-2	8.10	1.18	-0.52	5.9	108.3	74.5	-1.81	5.44	1.57
6669593	5.64e-2	8.05	1.18	0.55	5.9	253.3	107.1	-1.61	-5.44	-1.74
5990904	5.79e-2	8.10	1.18	-0.52	-5.4	291.2	108.9	-1.94	4.89	1.84
6661386	5.79e-2	8.05	1.18	0.55	-5.4	69.9	72.8	-1.75	-4.91	-1.60
CLE :		7.97	1.18	-0.49	6.3			-1.59	5.72	2.02

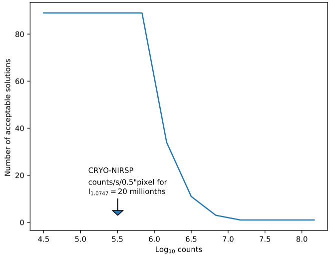

$$\chi^2 = \frac{1}{d-p-1}\left[\sum_{i=0,2}\frac{(S_i-O_i)^2}{\sigma_i^2} + \frac{(S_3-O_3)^2}{\sigma_3^2}\right]$$

- Solutions are degenerate in sets of 2.
- The number of degenerate solutions is a function of observation noise.
- Database resolution will also influence the quality of inverted parameters.
- The user should balance the database resolution to the noise influence in parameter accuracy.

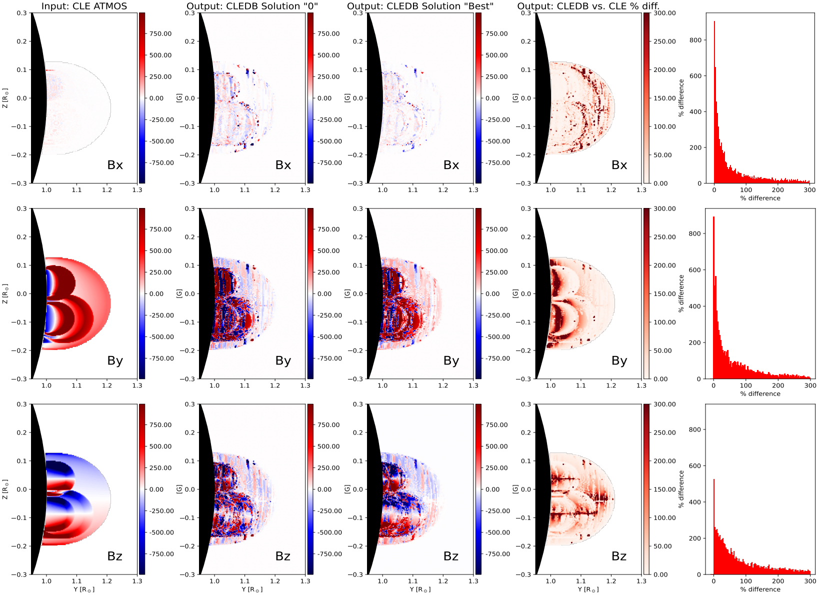
Input: CLE ATMOS
Output: CLEDB Solution "0"
Output: CLEDB Solution "Best"
Output: CLEDB vs. CLE % diff.
Bx
By
Bz
Z [R☉]
Y [R☉]
[G]
% difference

Preliminary application: IQU only vector magnetometry

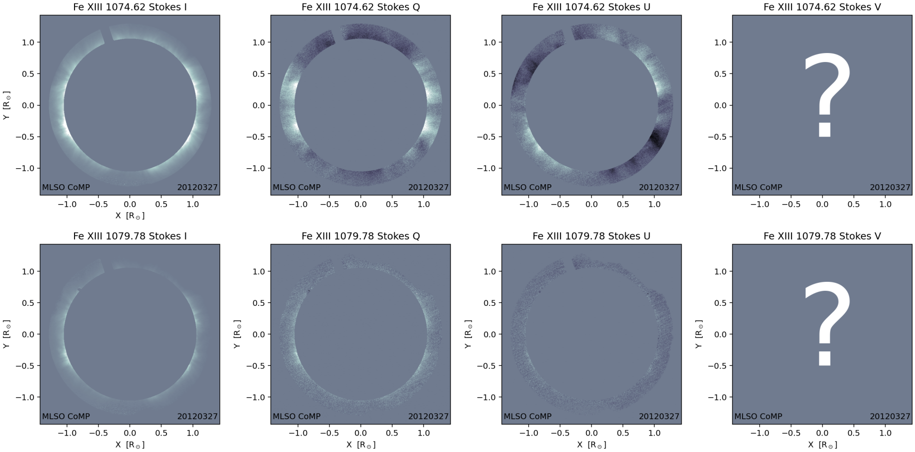

- MLSO CoMP Level 2 dataset of 27th March 2012.

Preliminary application: Coronal seismology with CoMP

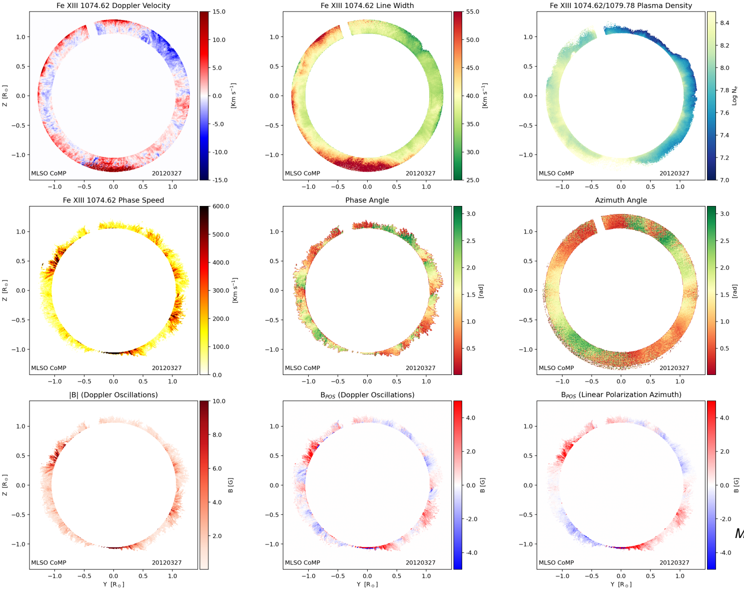

Morton et. al, 2016, NatComm
Yang et. al, 2020, Sci

Preliminary application: CoMP IQU Coronal inversion with CLEDB

For coronal magnetometry with CoMP see: Tomczyk,2007, Morton et. al, 2016, Yang et. al, 2020

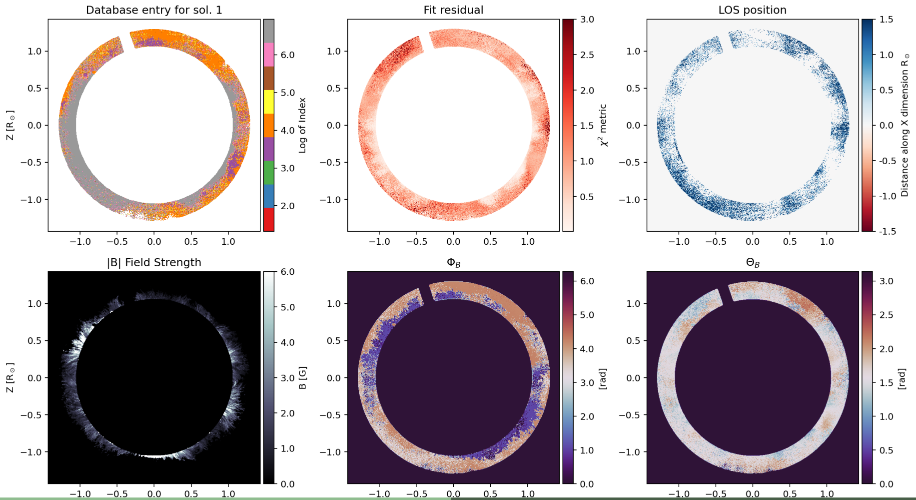

Preliminary application: CoMP IQU vector coronal magnetic field

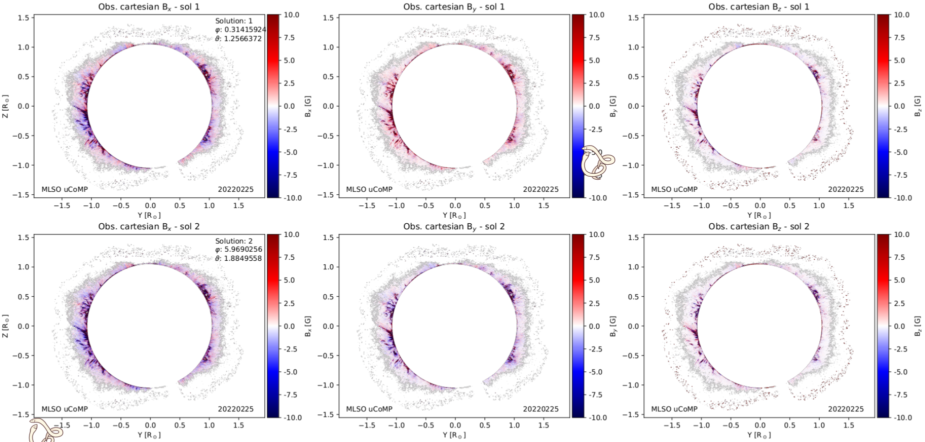

Paraschiv, 2023, in prep.

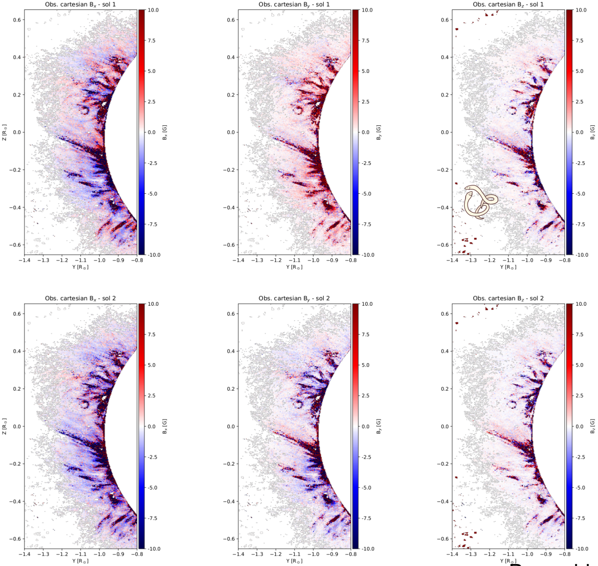

Paraschiv, 2023, in prep.

Main caveats and closing questions

- Eventual disambiguation of coronal vector magnetograms. CLEDB requires the sign of the magnetic field to fully remove additional degeneracies. HMI-like magnetogram are not yet achievable with DKIST LEV-2 data and/or CLEDB.
- Can we in practice combine lines from multiple atoms?
- Study PyCELP synergies.

- The current IQU implementation is a prototypwe and not yet available in the CLEDB repository.
- Complicated ARs and eruptive features are hard to recover using this implementation. IQU branch might be reliablly applicable to only synoptic use cases.
- A efficiency comparison when computing the azimuth via the phase angle vs. the linear polarization.

- It is important to estimate the densities and LOS locations of emitting plasma! Can we distinguish multiple emitting regions along the LOS?

- uCoMP and DKIST Cryo-NIRSP and DL-NIRSP CORONAL SCIENCE!

Do EXISTING CoMP DATASETS contain more untapped information regarding the REAL coronal magnetic field?

Thank you!

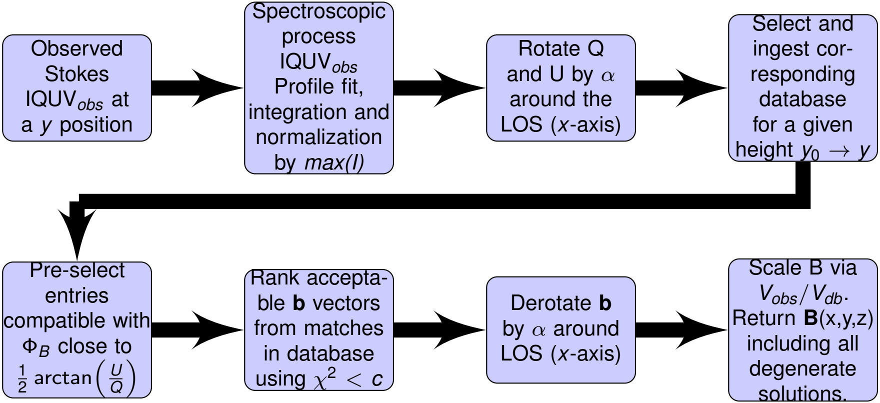

CLEDB is publicly available: https://github.com/arparaschiv/solar-coronal-inversion
Any independent tests and comments are welcome and appreciated!

arparaschiv@ucar.edu